Preprint
DOI 10.1007/s10915-017-0414-y

An Efficient Energy Minimization for Conformal Parameterizations

Mei-Heng Yueh · Wen-Wei Lin · Chin-Tien Wu · Shing-Tung Yau

Abstract Surface parameterizations have been widely applied to digital geometry processing. In this paper, we propose an efficient conformal energy minimization (CEM) algorithm for computing conformal parameterizations of simply-connected open surfaces with a very small angular distortion and a highly improved computational efficiency. In addition, we generalize the proposed CEM algorithm to computing conformal parameterizations of multiply-connected surfaces. Furthermore, we prove the existence of a nontrivial accumulation point of the proposed CEM algorithm under some mild conditions. Several numerical results show the efficiency and robustness of the CEM algorithm comparing to the existing state-of-the-art algorithms. An application of the CEM on the surface morphing between simply-connected open surfaces is demonstrated thereafter. Thanks to the CEM algorithm, the whole computations for the surface morphing can be performed efficiently and robustly.

Keywords Conformal Energy Minimization · Conformal Parameterizations · Simply-Connected Open Surfaces · Surface Morphing

Mathematics Subject Classification (2000) 15B48 · 52C26 · 65F05 · 65F30

1 Introduction

A surface parameterization is a bijective mapping that maps a surface to a simply shaped domain, which is called the parametric domain. The surface parameterization has been widely applied to tasks of digital geometry processing, such as surface registration, surface resampling, surface remeshing and surface texturing. It is usually difficult and time-consuming to carry out a task of geometry processing on a surface of a complicated geometrical structure. An appropriate parameterization for a surface can be applied to simplify the task via the one-to-one correspondence between the surface and the parametric domain. More details for methods and applications of surface parameterizations can be found in survey papers [7, 25, 14].

A good parameterization usually minimizes the distortion of either angles or areas. In particular, an angle-preserving map is also called a conformal parameterization. Some classical approaches for conformal parameterizations are:

1. Harmonic energy minimization [11, 21, 16, 17];
2. Laplacian operator linearization [1, 13];

Mei-Heng Yueh ✉ · Wen-Wei Lin · Chin-Tien Wu
Department of Applied Mathematics, National Chiao Tung University, Hsinchu 300, Taiwan
E-mail: mhyueh@math.nctu.edu.tw

Wen-Wei Lin
E-mail: wwlin@math.nctu.edu.tw

Chin-Tien Wu
E-mail: ctw@math.nctu.edu.tw

Shing-Tung Yau
Department of Mathematics, Harvard University, Cambridge, MA 02138, USA
E-mail: yau@math.harvard.edu

3. Angle-based flattening method [26, 24];
4. Circle packing method [27, 18].

In recent years, several efficient numerical methods for the computation of conformal parameterizations have been developed by different research groups. In the following, we briefly review the most related works for computing disk-shaped conformal parameterizations of simply-connected open surfaces. Gu and Yau [11] proposed an algorithm for computing conformal parameterizations via the heat diffusion on the double covered surface. Huang et al. [16] further improved the efficiency for convergence of the heat diffusion by applying the quasi-implicit Euler method. Choi and Lui [4] proposed an algorithm for computing conformal parameterizations based on the composition of Cayley transforms and quasiconformal maps. To further improve the efficiency of computations, Choi and Lui [5] developed a linear algorithm for computing conformal parameterizations based on the composition of a spherical conformal map [3, 10] of the double covered surface and a quasiconformal map. A detailed overview of previous works on different types of algorithms for computing conformal parameterizations can be found in [4, 5].

1.1 Contributions

In this paper, we propose an efficient conformal energy minimization (CEM) algorithm for computing conformal parameterizations of simply-connected open surfaces with a very small angular distortion and a highly improved computational efficiency. The contributions can be divided into three parts. First, we improve the conformality of the CEM by introducing a boundary iteration scheme. After the convergence of the boundary iteration, the conformal parameterization can be obtained by solving a harmonic map with the converged boundary map. Second, thanks to the technique of matrix computations, the proposed CEM is more efficient than the current existing state-of-the-art algorithms. As a result, the whole computational process of our developed algorithm is fast enough to be used in real applications. Third, we prove the existence of a nontrivial (nonconstant) accumulation point of the CEM under some mild conditions.

1.2 Notations and Overview

The following notations are frequently used in this paper. Other notations will be clearly defined whenever they appear.

- Bold letters, e.g. $\mathbf{u}$, $\mathbf{v}$, $\mathbf{w}$, denote vectors.
- Capital letters, e.g. A, B, C, denote matrices.
- Typewriter letters, e.g. $\mathtt{i}$, $\mathtt{j}$, $\mathtt{k}$, denote ordered sets of indices.
- i denotes the imaginary unit $\sqrt{-1}$.
- $n_{\mathbf{v}}$ denotes the number of elements of a vector $\mathbf{v}$.
- n_A denotes the number of rows of a square matrix A.
- $n_{\mathtt{i}}$ denotes the number of elements of an ordered index set $\mathtt{i}$.
- I_n denotes the identity matrix of size $n \times n$.
- $\mathbf{1}_n$ denotes the vector of length n with all entries being one.
- $\mathbf{0}$ denotes the zero vectors and matrices of appropriate sizes.
- $\mathbf{v}_i$ denotes the i-th entry of the vector $\mathbf{v}$.
- $\mathbf{v}_{\mathtt{i}}$ denotes the subvector of $\mathbf{v}$ composed of $\mathbf{v}_i$, for $i \in \mathtt{i}$.
- $|\mathbf{v}|$ denotes the vector with the i-th entry being $|\mathbf{v}_i|$.
- $\mathrm{diag}(\mathbf{v})$ denotes the diagonal matrix with the (i, i)-th entry being $\mathbf{v}_i$.
- $A_{i,j}$ denotes the (i, j)-th entry of the matrix A.
- $A_{\mathtt{i},\mathtt{j}}$ denotes the submatrix of A composed of $A_{i,j}$, for $i \in \mathtt{i}$ and $j \in \mathtt{j}$.

This paper is organized as follows. First, we introduce the discrete conformal maps in Section 2. Then, we describe the CEM algorithm in Section 3. We prove the existence of a nontrivial accumulation point for the CEM algorithm in Section 4. We present numerical results and comparisons with other methods in Section 5. Finally, we demonstrate an application of CEM on the surface morphing in Section 6. A concluding remark is given in Section 7.

2 Discrete Conformal Maps

A diffeomorphism $f : \mathcal{M} \to \mathcal{N}$ between two Riemann surfaces is said to be conformal if it satisfies $f^* \, \mathrm{d}s_{\mathcal{N}}^2 = \lambda \, \mathrm{d}s_{\mathcal{M}}^2$ with some positive scalar function λ, where $\mathrm{d}s_{\mathcal{M}}^2$ and $\mathrm{d}s_{\mathcal{N}}^2$ are the first fundamental forms of surfaces $\mathcal{M}$ and $\mathcal{N}$, respectively, and $f^* \, \mathrm{d}s_{\mathcal{N}}^2$ is the pullback metric induced by f. Here, the scaling factor λ is known as the conformal factor with respect to the conformal map f. The uniformization theorem [28] tells that every simply-connected open surface $\mathcal{M}$ is conformally equivalent to a unit disk $\mathbb{D} \subset \mathbb{C}$. That is, there exists a conformal map f that maps the surface $\mathcal{M}$ to a unit disk $\mathbb{D}$. Our goal is to efficiently compute such a conformal map f with small angular distortions.

In the following, we briefly describe the computations of conformal maps via the Dirichlet energy minimization. Let $\mathcal{M}$ be a Riemann surface in $\mathbb{R}^3$. The *Dirichlet energy functional* [11] for a smooth map $f : \mathcal{M} \to \mathbb{D}$ is defined by

$$\mathcal{E}_D(f) = \frac{1}{2} \int_{\mathcal{M}} \|\nabla f\|^2 \, \mathrm{d}v_{\mathcal{M}}, \tag{1}$$

where $dv_{\mathcal{M}}$ is the area element of the surface $\mathcal{M}$. Let $\mathcal{A}(f)$ measure the area of the image $f(\mathcal{M})$. The *conformal energy* of f is defined by

$$\mathcal{E}_C(f) = \mathcal{E}_D(f) - \mathcal{A}(f). \tag{2}$$

It is known that $\mathcal{E}_D(f) \geq \mathcal{A}(f)$, and the equality holds if and only if f is a conformal map [19, 6]. When the image $f(\mathcal{M})$ is the unit disk $\mathbb{D}$, the area of the image would be a constant $\mathcal{A}(f) = \pi$. As a result, a conformal map to the unit disk is actually a minimizer for the Dirichlet energy functional defined by Eq. (1) under a circular boundary constraint. In other words, the desired conformal map f is a minimizer for the optimization problem

$$f = \operatorname*{argmin}_{g : \mathcal{M} \to \mathbb{D}} \{ \mathcal{E}_D(g) \mid g|_{\partial\mathcal{M}} : \partial\mathcal{M} \to \partial\mathbb{D} \text{ and } g(\mathcal{M}) = \mathbb{D} \}. \tag{3}$$

It is well-known that every conformal map is harmonic [7]. Once the boundary condition $f|_{\partial\mathcal{M}} = f_b : \partial\mathcal{M} \to \partial\mathbb{D}$ is given, the map f can be obtained by solving a Laplace-Beltrami equation

$$\begin{cases} \triangle_{\mathcal{M}} f = 0 & \text{on } \mathcal{M} \backslash \partial\mathcal{M}, \\ f|_{\partial\mathcal{M}} = f_b, \end{cases} \tag{4}$$

where $\triangle_{\mathcal{M}}$ is the Laplace-Beltrami operator [22, 23]. Hence the map f is uniquely determined by the boundary condition f_b in Eq. (4). However, in general, it is difficult to find the optimal boundary condition f_b, since there are infinitely many possible choices for boundary maps.

Remark 1 The solution to Eq. (4) is known as a *harmonic map*, which is a minimizer of the Dirichlet energy functional (1) under a given boundary constraint $f|_{\partial\mathcal{M}} = f_b$.

In the linear discretization, the surface $\mathcal{M}$ we considered is a Delaunay triangulation mesh [11] with n vertices in a certain order. A triangular mesh usually satisfies the conditions stated in Definition 1. Otherwise, a remeshing process can be applied to reach the conditions.

Definition 1 (Well-conditioned mesh) A triangular mesh $\mathcal{M}$ for a simply-connected open surface is said to be *well-conditioned* if it satisfies the following conditions:

(i) The graph of $\mathcal{M}$ is connected.
(ii) The subgraph on all the interior vertices is connected.
(iii) The subgraph on all the boundary vertices is connected.
(iv) Every boundary vertex is connected to at least one interior vertex.

Hereafter, we suppose that $\mathcal{M}$ is a well-conditioned Delaunay triangulation mesh. A piecewise linear approximation of the map $f : \mathcal{M} \to \mathbb{D}$ can be expressed by a complex-valued vector $\mathbf{f} = (\mathbf{f}_1, \ldots \mathbf{f}_n)^\top \in \mathbb{C}^n$, where $\mathbf{f}_k = \mathbf{u}_k + \mathrm{i}\mathbf{v}_k$, for $k = 1, \ldots, n$. Then the discrete Dirichlet energy [11] can be written as

$$\mathcal{E}_D(\mathbf{f}) = \frac{1}{2} \sum_{[i,\, j] \in \text{edges}} \frac{\cot\alpha_{ij} + \cot\alpha_{ji}}{2} |\mathbf{f}_i - \mathbf{f}_j|^2 = \frac{1}{2} \mathbf{f}^* L \mathbf{f}, \tag{5}$$

where α_{ij} and α_{ji} are the two angles opposite to the edge $[i,j]$ connecting vertices i and j on the mesh $\mathcal{M}$, and L is the discrete Laplacian matrix defined by

$$L_{i,j} = \begin{cases} -\frac{1}{2}(\cot\alpha_{ij} + \cot\alpha_{ji}) & \text{if } [i,j] \text{ is an edge, } j \neq i, \\ -\sum_{k\neq i} L_{i,k} & \text{if } j = i, \\ 0 & \text{otherwise.} \end{cases} \tag{6}$$

Note that for a Delaunay triangular mesh, the entry $L_{i,j} < 0$ if $[i,j]$ is an edge.

Similarly, the discrete conformal energy is defined by

$$\mathcal{E}_C(\mathbf{f}) = \mathcal{E}_D(\mathbf{f}) - \mathcal{A}(\mathbf{f}), \tag{7}$$

where the area of the image $\mathcal{A}(\mathbf{f})$ is defined by

$$\mathcal{A}(\mathbf{f}) = \frac{1}{2} \sum_{[i,j]\in\partial\mathcal{M}} (\mathbf{u}_i\mathbf{v}_j - \mathbf{u}_j\mathbf{v}_i). \tag{8}$$

By a certain reordering of the indices of vertices, the matrix L and the complex-valued vector $\mathbf{f}$ can be written as

$$L = \begin{bmatrix} L_{\mathtt{i},\mathtt{i}} & L_{\mathtt{i},\mathtt{b}} \\ L_{\mathtt{i},\mathtt{b}}^\top & L_{\mathtt{b},\mathtt{b}} \end{bmatrix} \quad \text{and} \quad \mathbf{f} = \begin{bmatrix} \mathbf{f}_{\mathtt{i}} \\ \mathbf{f}_{\mathtt{b}} \end{bmatrix}, \tag{9}$$

respectively, where $\mathtt{i}$ and $\mathtt{b}$ denote the ordered index sets of the interior vertices and the boundary vertices of the triangular mesh $\mathcal{M}$, respectively. Then the discrete Laplace-Beltrami equation can be expressed as a linear system

$$L_{\mathtt{i},\mathtt{i}}\mathbf{f}_{\mathtt{i}} = -L_{\mathtt{i},\mathtt{b}}\mathbf{f}_{\mathtt{b}}, \tag{10}$$

where $\mathbf{f}_{\mathtt{b}}$ is a given boundary condition. More details on topics of theoretical and computational conformal geometry can be found in [9, 11, 12].

3 Conformal Energy Minimization Algorithm

In this section, we describe our CEM algorithm for computing a conformal parameterization f of a simply-connected open surface $\mathcal{M}$. In Section 3.1, we introduce an appropriate initial boundary map obtained by computing a harmonic map with a fixed triangle as a constraint. To minimize the conformal energy of the map f defined in Eq. (2), we introduce an iteration scheme to improve the boundary map in Section 3.2. When a satisfactory boundary map is convergent, the conformal parameterization of the surface $\mathcal{M}$ can be obtained by solving a Laplace-Beltrami equation of the form (4) with a certain boundary condition.

3.1 Initial Boundary Maps for CEM Algorithm

The initial boundary map f_b in Eq. (4) can be obtained by solving the Laplace-Beltrami equation proposed by Angenent et al. [1, 13]

$$\triangle_{\mathcal{M}} f = \left(\frac{\partial}{\partial u} - \mathrm{i}\frac{\partial}{\partial v}\right)\delta_p, \tag{11}$$

where δ_p is the Dirac delta function at p. Here, p is a selected point on $\mathcal{M}$ and (u,v) is the local coordinate defined on a neighborhood of p. This method is originally designed for the computation of the conformal equivalence $f : \Sigma\backslash\{p\} \to \mathbb{C}$ for the genus-zero closed surface Σ. Similarly, for the simply-connected open surface $\mathcal{M}$, a map

$$f : \mathcal{M}\backslash\{p\} \to \mathbb{C}\backslash\Omega \tag{12}$$

can be obtained by solving Eq. (11). Here $\partial\Omega$ is the natural boundary resulted from Eq. (11). Although the map f in (12) is not guaranteed to be conformal, several numerical experiments indicate that the angular distortion of the map f in (12) is relatively large around the neighborhood of p. Based on these observations, the point p can be automatically selected closest to the mass center of the mesh $\mathcal{M}$ so that the angular distortion is relatively small on the boundary $\partial\mathcal{M}$.

In the linear discretization, the neighborhood of p is given by a triangular element $[a,b,c]$ with respect to the vertices $\{p_a,p_b,p_c\}$ on the mesh $\mathcal{M}$. The Laplace-Beltrami equation (11) can be efficiently solved by the linear system

$$L\mathbf{f} = \mathbf{b}, \tag{13}$$

where the matrix L is the discrete Laplacian matrix defined by Eq. (6), and the vector $\mathbf{b} = (\mathbf{b}_1,\ldots,\mathbf{b}_n)^\top$ is given by

$$\mathbf{b}_k := \begin{cases} 0 & \text{if } k \notin \{a,b,c\}, \\ \frac{-1}{\|p_b-p_a\|_2} + \mathrm{i}\frac{1-\alpha}{\|p_c-(p_a+\alpha(p_b-p_a))\|_2} & \text{if } k = a, \\ \frac{1}{\|p_b-p_a\|} + \mathrm{i}\frac{\alpha}{\|p_c-(p_a+\alpha(p_b-p_a))\|_2} & \text{if } k = b, \\ \mathrm{i}\frac{-1}{\|p_c-(p_a+\alpha(p_b-p_a))\|_2} & \text{if } k = c \end{cases} \tag{14}$$

with $\alpha = \frac{\langle p_c-p_a, p_b-p_a\rangle}{\|p_b-p_a\|_2^2}$. Then, the new initial discrete boundary map can be updated by the original $\mathbf{f}_\mathtt{b}$ after performing the centralization

$$\mathbf{f}_\mathtt{b} \leftarrow \left(I_{n_\mathtt{b}} - \frac{\mathbf{1}_{n_\mathtt{b}}\mathbf{1}_{n_\mathtt{b}}^\top}{n_\mathtt{b}}\right)\mathbf{f}_\mathtt{b} \tag{15}$$

and the normalization

$$\mathbf{f}_\mathtt{b} \leftarrow \left(\operatorname{diag}\left(|\mathbf{f}_\mathtt{b}|\right)\right)^{-1}\mathbf{f}_\mathtt{b}. \tag{16}$$

Note that the discrete Laplacian matrix L is singular. So the linear system (13) is a singular system that has infinitely many solutions. In fact, according to the definition of a discrete Laplacian matrix in (6), it is clear that $\ker(L) = \operatorname{span}\{\mathbf{1}_n\}$ since the sum of each row of L is zero. As a result, if $\mathbf{g}$ is a solution to the linear system (13), $\mathbf{g} + z\mathbf{1}_n$ is also a solution, for every $z \in \mathbb{C}$. Intuitively, it is expected that the singular linear system (13) can be reduced into a nonsingular one by fixing one point of the solution. In the following, we give a concrete statement in Theorem 1. For convenience, we give the definition of an M-matrix [2] and the related lemma.

Definition 2 (i) A matrix $A \in \mathbb{R}^{m\times n}$ is said to be nonnegative (positive) if all entries of A are nonnegative (positive).
(ii) A matrix $A \in \mathbb{R}^{n\times n}$ is said to be an M-matrix if $A = sI - B$, where B is nonnegative and $s \geq \rho(B)$.

Lemma 1 (Theorem 1.4.10 in [20]) *Suppose $A \in \mathbb{R}^{n\times n}$ is a singular, irreducible M-matrix. Then each principal submatrix of A other than A itself is a nonsingular M-matrix.*

Lemma 2 *The $n \times n$ matrix L defined in (6), is a singular M-matrix.*

Proof By the definition of the matrix L in (6), each row sum of L is zero. Hence $L\mathbf{1}_n = \mathbf{0}$, and therefore L is singular. To show that L is an M-matrix, we write $L = sI_n - B$, where $s = \max_{1\leq i\leq n}(L_{i,i})$ and $B = sI_n - L$. According to the definition of L, it holds that $L_{i,i} = -\sum_{k\neq i} L_{i,k}$, for $i = 1,\ldots,n$. Hence, by the Gershgorin circle theorem [8], we have $s \geq \rho(B)$. Therefore, the matrix L is an M-matrix by Definition 2 (ii). □

In practice, for solving a Laplacain linear system of (13), the technique stated in the following theorem can be applied.

Theorem 1 *Let L be an $n \times n$ Laplacian matrix of the mesh $\mathcal{M}$ as in (6). Then the linear system $L\mathbf{f} = \mathbf{b}$ in (13) can be reduced into a nonsingular one by removing the k-th entries of the vectors $\mathbf{f}$ and $\mathbf{b}$, and the k-th row and column of L, respectively. Here the index k can be chosen as any number in $\{1,\ldots,n\}$.*

Proof Without loss of generality, we set $k = n$. Let $\mathbf{g} = (g_1,\ldots g_n)^\top$ be a solution to (13). Then $\mathbf{g} - g_n\mathbf{1}_n$ is also a solution. That is,

$$\begin{bmatrix} L_{\mathtt{u},\mathtt{u}} & L_{\mathtt{u},n} \\ L_{\mathtt{u},n}^\top & L_{n,n} \end{bmatrix} \begin{bmatrix} \mathbf{g}_\mathtt{u} - g_n\mathbf{1}_{n_\mathtt{u}} \\ 0 \end{bmatrix} = \begin{bmatrix} \mathbf{b}_\mathtt{u} \\ b_n \end{bmatrix}, \tag{17}$$

where $\mathtt{u}$ is the index set $\{1,\ldots,n-1\}$. From (17) we have

$$L_{\mathtt{u},\mathtt{u}}(\mathbf{g}_\mathtt{u} - g_n\mathbf{1}_{n_\mathtt{u}}) = \mathbf{b}_\mathtt{u}, \tag{18}$$

$$L_{\mathtt{u},n}^\top(\mathbf{g}_\mathtt{u} - g_n\mathbf{1}_{n_\mathtt{u}}) = b_n. \tag{19}$$

Because of the connectivity of the mesh $\mathcal{M}$ and Lemma 2, L is an irreducible and singular M-matrix. By applying Lemma 1, the matrix $L_{\mathtt{u},\mathtt{u}}$ is nonsingular. So the solution to the linear system (18) is unique. Hence Eq. (19) would always hold and can be removed. Therefore, solving the singular system $L\mathbf{f} = \mathbf{b}$ is equivalent to solving the nonsingular system $L_{\mathtt{u},\mathtt{u}}\mathbf{f}_{\mathtt{u}} = \mathbf{b}_{\mathtt{u}}$ by setting $f_n = 0$. $\square$

On the other hand, the vector $\mathbf{b}$ in the linear system (13) contains only three nonzero entries. As a result, the linear system (13) can be written as

$$\begin{bmatrix} L_{\mathtt{v},\mathtt{v}} & L_{\mathtt{v},\mathtt{w}} \\ L_{\mathtt{v},\mathtt{w}}^\top & L_{\mathtt{w},\mathtt{w}} \end{bmatrix} \begin{bmatrix} \mathbf{f}_{\mathtt{v}} \\ \mathbf{f}_{\mathtt{w}} \end{bmatrix} = \begin{bmatrix} \mathbf{0} \\ \mathbf{b}_{\mathtt{w}} \end{bmatrix}, \tag{20}$$

where the index sets $\mathtt{w} = \{a, b, c\}$ and $\mathtt{v} = \{1, \ldots, n\} \backslash \{a, b, c\}$, respectively. Note that the matrix L can be decomposed as

$$\begin{bmatrix} L_{\mathtt{v},\mathtt{v}} & L_{\mathtt{v},\mathtt{w}} \\ L_{\mathtt{v},\mathtt{w}}^\top & L_{\mathtt{w},\mathtt{w}} \end{bmatrix} = \begin{bmatrix} I_{n_{\mathtt{v}}} & L_{\mathtt{v},\mathtt{w}} L_{\mathtt{w},\mathtt{w}}^{-1} \\ & I_{n_{\mathtt{w}}} \end{bmatrix} \begin{bmatrix} S_{L_{\mathtt{w},\mathtt{w}}} & \\ & L_{\mathtt{w},\mathtt{w}} \end{bmatrix} \begin{bmatrix} I_{n_{\mathtt{v}}} & \\ L_{\mathtt{w},\mathtt{w}}^{-1} L_{\mathtt{v},\mathtt{w}}^\top & I_{n_{\mathtt{w}}} \end{bmatrix},$$

where $S_{L_{\mathtt{w},\mathtt{w}}} = L_{\mathtt{v},\mathtt{v}} - L_{\mathtt{v},\mathtt{w}} L_{\mathtt{w},\mathtt{w}}^{-1} L_{\mathtt{v},\mathtt{w}}^\top$ is the Schur complement of the block $L_{\mathtt{w},\mathtt{w}}$. By applying the inverse formula for block matrices, the inverse of the matrix L can be expressed as

$$\begin{bmatrix} L_{\mathtt{v},\mathtt{v}} & L_{\mathtt{v},\mathtt{w}} \\ L_{\mathtt{v},\mathtt{w}}^\top & L_{\mathtt{w},\mathtt{w}} \end{bmatrix}^{-1} = \begin{bmatrix} I_{n_{\mathtt{v}}} & \\ -L_{\mathtt{w},\mathtt{w}}^{-1} L_{\mathtt{v},\mathtt{w}}^\top & I_{n_{\mathtt{w}}} \end{bmatrix} \begin{bmatrix} S_{L_{\mathtt{w},\mathtt{w}}}^{-1} & \\ & L_{\mathtt{w},\mathtt{w}}^{-1} \end{bmatrix} \begin{bmatrix} I_{n_{\mathtt{v}}} & -L_{\mathtt{v},\mathtt{w}} L_{\mathtt{w},\mathtt{w}}^{-1} \\ & I_{n_{\mathtt{w}}} \end{bmatrix}.$$

Therefore, the solution $\mathbf{f}$ can be written as

$$\begin{aligned} \begin{bmatrix} \mathbf{f}_{\mathtt{v}} \\ \mathbf{f}_{\mathtt{w}} \end{bmatrix} &= \begin{bmatrix} I_{n_{\mathtt{v}}} & \\ -L_{\mathtt{w},\mathtt{w}}^{-1} L_{\mathtt{v},\mathtt{w}}^\top & I_{n_{\mathtt{w}}} \end{bmatrix} \begin{bmatrix} S_{L_{\mathtt{w},\mathtt{w}}}^{-1} & \\ & L_{\mathtt{w},\mathtt{w}}^{-1} \end{bmatrix} \begin{bmatrix} I_{n_{\mathtt{v}}} & -L_{\mathtt{v},\mathtt{w}} L_{\mathtt{w},\mathtt{w}}^{-1} \\ & I_{n_{\mathtt{w}}} \end{bmatrix} \begin{bmatrix} \mathbf{0} \\ \mathbf{b}_{\mathtt{w}} \end{bmatrix} \\ &= \begin{bmatrix} -S_{L_{\mathtt{w},\mathtt{w}}}^{-1} L_{\mathtt{v},\mathtt{w}} L_{\mathtt{w},\mathtt{w}}^{-1} \mathbf{b}_{\mathtt{w}} \\ L_{\mathtt{w},\mathtt{w}}^{-1} \left(\mathbf{b}_{\mathtt{w}} + L_{\mathtt{v},\mathtt{w}}^\top S_{L_{\mathtt{w},\mathtt{w}}}^{-1} L_{\mathtt{v},\mathtt{w}} L_{\mathtt{w},\mathtt{w}}^{-1} \mathbf{b}_{\mathtt{w}} \right) \end{bmatrix} \\ &= \begin{bmatrix} -S_{L_{\mathtt{w},\mathtt{w}}}^{-1} L_{\mathtt{v},\mathtt{w}} L_{\mathtt{w},\mathtt{w}}^{-1} \mathbf{b}_{\mathtt{w}} \\ L_{\mathtt{w},\mathtt{w}}^{-1} \left(\mathbf{b}_{\mathtt{w}} - L_{\mathtt{v},\mathtt{w}}^\top \mathbf{f}_{\mathtt{v}} \right) \end{bmatrix}. \end{aligned}$$

Consequently, the linear system (20) can be reduced into the form as

$$S_{L_{\mathtt{w},\mathtt{w}}} \mathbf{f}_{\mathtt{v}} = -L_{\mathtt{v},\mathtt{w}} L_{\mathtt{w},\mathtt{w}}^{-1} \mathbf{b}_{\mathtt{w}}. \tag{21}$$

Here the linear system (21) can be solved by the Sherman-Morrison-Woodbury formula. After $\mathbf{f}_{\mathtt{v}}$ is obtained by (21), $\mathbf{f}_{\mathtt{w}}$ can then be computed by solving the linear system

$$L_{\mathtt{w},\mathtt{w}} \mathbf{f}_{\mathtt{w}} = \mathbf{b}_{\mathtt{w}} - L_{\mathtt{v},\mathtt{w}}^\top \mathbf{f}_{\mathtt{v}}.$$

In general, the linear systems (18) and (21) are mathematically equivalent. However, in our numerical experiences, solving Eq. (18) is slightly more efficient than Eq. (21). So, in our CEM algorithm, we adopt Eq. (18) instead of Eq. (21).

3.2 Boundary Iteration Scheme for CEM Algorithm

To further improve the boundary map, we propose a boundary iteration scheme. First, the map of interior vertices is updated by solving the linear system

$$L_{\mathtt{i},\mathtt{i}} \mathbf{f}_{\mathtt{i}}^{(k)} = -L_{\mathtt{i},\mathtt{b}} \mathbf{f}_{\mathtt{b}}^{(k)}. \tag{22}$$

Then the map of boundary vertices is updated by solving the linear system

$$L_{\mathtt{b},\mathtt{b}} \mathbf{f}_{\mathtt{b}}^{(k+1)} = -L_{\mathtt{b},\mathtt{i}} \mathbf{f}_{\mathtt{i}}^{(k)}. \tag{23}$$

To guarantee the boundary map is always on the unit circle, we perform the centralization

$$\mathbf{f}_{\mathtt{b}}^{(k+1)} \leftarrow \left(I_{n_{\mathtt{b}}} - \frac{\mathbf{1}_{n_{\mathtt{b}}} \mathbf{1}_{n_{\mathtt{b}}}^\top}{n_{\mathtt{b}}} \right) \mathbf{f}_{\mathtt{b}}^{(k+1)}, \tag{24}$$

and the normalization to the boundary map

$$\mathbf{f}_{\mathtt{b}}^{(k+1)} \leftarrow \left(\operatorname{diag}\left(\left|\mathbf{f}_{\mathtt{b}}^{(k+1)}\right|\right)\right)^{-1} \mathbf{f}_{\mathtt{b}}^{(k+1)}. \tag{25}$$

Equivalently, the iterations (22)-(25) for the boundary map can be expressed as

$$\mathbf{f}_{\mathtt{b}}^{(k+1)} = \left(N_{\mathtt{b}}^{(k)}\right)^{-1} CK\mathbf{f}_{\mathtt{b}}^{(k)}, \tag{26}$$

where K is defined by

$$K = L_{\mathtt{b},\mathtt{b}}^{-1} L_{\mathtt{i},\mathtt{b}}^{\top} L_{\mathtt{i},\mathtt{i}}^{-1} L_{\mathtt{i},\mathtt{b}}, \tag{27}$$

the centralization and the normalization matrices C and $N_{\mathtt{b}}^{(k)}$ are, respectively, given by

$$C = I_{n_{\mathtt{b}}} - \frac{\mathbf{1}_{n_{\mathtt{b}}} \mathbf{1}_{n_{\mathtt{b}}}^{\top}}{n_{\mathtt{b}}} \tag{28}$$

and

$$N_{\mathtt{b}}^{(k)} = \operatorname{diag}\left(\left|CK\mathbf{f}_{\mathtt{b}}^{(k)}\right|\right). \tag{29}$$

Remark 2 The algebraic meaning for the centralization matrix C is actually a deflating transformation on the matrix K, i.e., the matrix C deflates the eigenvalue 1 of K to 0 while preserving the other eigenvalues unchanged. On the other hand, C transforms each eigenvector $\mathbf{v}$ of K to $C\mathbf{v}$. That is,

$$(CK)\mathbf{1}_{n_{\mathtt{b}}} = \mathbf{0},$$

and

$$(CK)(C\mathbf{v}) = \lambda C\mathbf{v},$$

for every eigenvalue $\lambda \neq 1$.

Remark 3 Numerical experiments indicate that an inversion for modifying $\mathbf{f}_{\mathtt{i}}^{(k)}$ in Eq. (23) by $\left(\operatorname{diag}\left(\left|\mathbf{f}_{\mathtt{i}}^{(k)}\right|\right)\right)^{-2} \mathbf{f}_{\mathtt{i}}^{(k)}$ would have a better convergence in the iterations (22)-(25). In practice, Eq. (23) is replaced by the equation

$$L_{\mathtt{b},\mathtt{b}} \mathbf{f}_{\mathtt{b}}^{(k+1)} = -L_{\mathtt{b},\mathtt{i}} \left(\operatorname{diag}\left(\left|\mathbf{f}_{\mathtt{i}}^{(k)}\right|\right)\right)^{-2} \mathbf{f}_{\mathtt{i}}^{(k)}. \tag{30}$$

Then, the conformal energy of the map $\mathcal{E}_C(\mathbf{f}_{\mathtt{b}}^{(k)})$ in the iterations (22), (30), (24) (25) would become monotonically decreasing.

The CEM algorithm is summarized in Algorithm 1 in detail.

Algorithm 1 Conformal Energy Minimization (CEM)

Input: A triangular mesh $\mathcal{M}$ of a simply-connected open surface.
Output: A conformal parameterization $\mathbf{f} : \mathcal{M} \to \mathbb{D}$.

Classify the vertices of $\mathcal{M}$ into two groups:

$$\mathtt{i} = \{\text{indices of interior vertices}\} \text{ and } \mathtt{b} = \{\text{indices of boundary vertices}\}.$$

Solve the linear system $L\mathbf{f} = \mathbf{b}$ by setting $f_n = 0$, where L and $\mathbf{b}$ are defined by Eq. (6) and Eq. (13), respectively.
Centralize $\mathbf{f}_{\mathtt{b}} \leftarrow \left(I_{n_{\mathtt{b}}} - \frac{\mathbf{1}_{n_{\mathtt{b}}} \mathbf{1}_{n_{\mathtt{b}}}^{\top}}{n_{\mathtt{b}}}\right) \mathbf{f}_{\mathtt{b}}$.
Normalize $\mathbf{f}_{\mathtt{b}} \leftarrow (\operatorname{diag}(|\mathbf{f}_{\mathtt{b}}|))^{-1} \mathbf{f}_{\mathtt{b}}$.
Solve the linear system $L_{\mathtt{i},\mathtt{i}} \mathbf{f}_{\mathtt{i}} = -L_{\mathtt{i},\mathtt{b}} \mathbf{f}_{\mathtt{b}}$.
while not convergent **do**
  Solve the linear system $L_{\mathtt{b},\mathtt{b}} \mathbf{f}_{\mathtt{b}} = -L_{\mathtt{b},\mathtt{i}} (\operatorname{diag}(|\mathbf{f}_{\mathtt{i}}|))^{-2} \mathbf{f}_{\mathtt{i}}$.
  Centralize $\mathbf{f}_{\mathtt{b}} \leftarrow \left(I_{n_{\mathtt{b}}} - \frac{\mathbf{1}_{n_{\mathtt{b}}} \mathbf{1}_{n_{\mathtt{b}}}^{\top}}{n_{\mathtt{b}}}\right) \mathbf{f}_{\mathtt{b}}$.
  Normalize $\mathbf{f}_{\mathtt{b}} \leftarrow (\operatorname{diag}(|\mathbf{f}_{\mathtt{b}}|))^{-1} \mathbf{f}_{\mathtt{b}}$.
  Solve the linear system $L_{\mathtt{i},\mathtt{i}} \mathbf{f}_{\mathtt{i}} = -L_{\mathtt{i},\mathtt{b}} \mathbf{f}_{\mathtt{b}}$.
end while

3.3 Generalization of CEM to Multiply-Connected Surfaces

To generalize the proposed CEM algorithm, we apply Koebe's method proposed by Zeng et al. [29, 30] for computing conformal parameterizations of multiply-connected surfaces. Given a surface $\mathcal{M}$ with multiple holes, the generalized CEM algorithm is aimed to find a conformal map f that maps $\mathcal{M}$ to a unit disk with circular holes. The existence of such a conformal map f is guaranteed by Koebe's uniformization theory. To illustrate the procedure of the generalized CEM algorithm, we suppose a surface $\mathcal{M}$ has 4 boundaries

$$\partial\mathcal{M} = \gamma_0 - \gamma_1 - \gamma_2 - \gamma_3,$$

as shown in Fig. 1 (a). Each boundary γ_i except γ_3 is filled by a patch $\mathcal{P}_i$ composed of a vertex c_i at the centroid of γ_i and the edges connecting the vertex c_i to the vertices on γ_i, for $i = 0, 1, 2$. Then

$$\mathcal{M}^{(3)} \equiv \mathcal{M} \cup \mathcal{P}_0 \cup \mathcal{P}_1 \cup \mathcal{P}_2$$

is a simply-connected open surface so that a conformal map $f_3 : \mathcal{M}^{(3)} \to \mathbb{D}$ can be obtained by the CEM algorithm. The image of $f_3(\mathcal{M})$ is shown in Fig. 1 (b). Next, we map the centroid of γ_2 to the infinity by an inversion $\varphi_2(z) = (z - c_2)^{-1}$, as shown in Fig. 1 (c). Similarly, we fill up all holes except γ_2 and form a simply-connected open surface $\mathcal{M}^{(2)}$ so that a conformal map $f_2 : \mathcal{M}^{(2)} \to \mathbb{D}$ can be obtained by the CEM algorithm, as shown in Fig. 1 (d). Continue these steps as illustrated in Fig. 1 (e)-(h) until every boundary is mapped to a circle. The desired conformal parameterization of the multiply-connected surface $\mathcal{M}$ is then given by

$$f \equiv f_0 \circ \varphi_0 \circ f_1 \circ \varphi_1 \circ f_2 \circ \varphi_2 \circ f_3.$$

We summarize the generalized CEM algorithm for multiply-connected surfaces in Algorithm 2.

Algorithm 2 Generalized CEM for Multiply-Connected Surfaces

Input: A triangular mesh $\mathcal{M}$ of a multiply-connected surface.
Output: A conformal parameterization $\mathbf{f} : \mathcal{M} \to \mathbb{D}$.

1: Find the boundaries $\partial\mathcal{M} = \gamma_0 - \sum_{i=1}^{n} \gamma_i$.
2: Fill up all holes except γ_n and obtain a simply-connected open surface $\mathcal{M}^{(n)}$.
3: Compute $\mathbf{f} : \mathcal{M}^{(n)} \to \mathbb{D}$ by CEM algorithm 1.
4: Open all holes $\mathbf{f} \leftarrow \mathbf{f}(\mathcal{M})$.
5: **for** $i = n-1, \ldots, 0$ **do**
6:     Compute the centroid c_i of the boundary γ_i.
7:     Do inversion $\mathbf{f}_j \leftarrow (\mathbf{f}_j - c_i)^{-1}$, $j = 1, \ldots, n_{\mathbf{f}}$.
8:     Fill up all holes except γ_i and obtain a simply-connected open surface $\mathcal{M}^{(i)}$.
9:     Compute $\mathbf{f} : \mathcal{M}^{(i)} \to \mathbb{D}$ by CEM algorithm 1.
10:     Open all holes $\mathbf{f} \leftarrow \mathbf{f}(\mathcal{M})$.
11: **end for**

---

4 Existence of a Nontrivial Accumulation Point

The aim of this section is to prove the existence of a nontrivial (nonconstant) accumulation point of the sequence $\{\mathbf{f}_{\mathtt{b}}^{(k)}\}_{k\in\mathbb{N}}$, defined by (26), when the initial vector $\mathbf{f}_{\mathtt{b}}^{(0)} \neq z\mathbf{1}_{n_{\mathtt{b}}}$ for any $z \in \mathbb{C}$. To exclude the rotations that may occur in the iteration (26), we set $(\mathbf{f}_{\mathtt{b}}^{(k)})_1 = 1$, for every $k \in \mathbb{N}$. We first introduce some useful lemmas related to M-matrices.

Lemma 3 (Theorem 1.4.7 in [20]) *If $A \in \mathbb{R}^{n\times n}$ is a nonsingular M-matrix, then A^{-1} is a nonnegative matrix. Moreover, if A is irreducible, then A^{-1} is a positive matrix.*

Lemma 4 (Perron Theorem [15]) *Let $A \in \mathbb{R}^{n\times n}$ be a positive matrix. Then*

(i) $\rho(A)$ is an eigenvalue of A, and all the other eigenvalues are strictly smaller than $\rho(A)$ in modulus.
(ii) $\rho(A)$ is the only eigenvalue that has a positive eigenvector.
(iii) $\rho(A)$ has algebraic multiplicity one.

The following theorem plays a crucial role in the geometric understanding of the iteration matrix defined by Eq. (27).

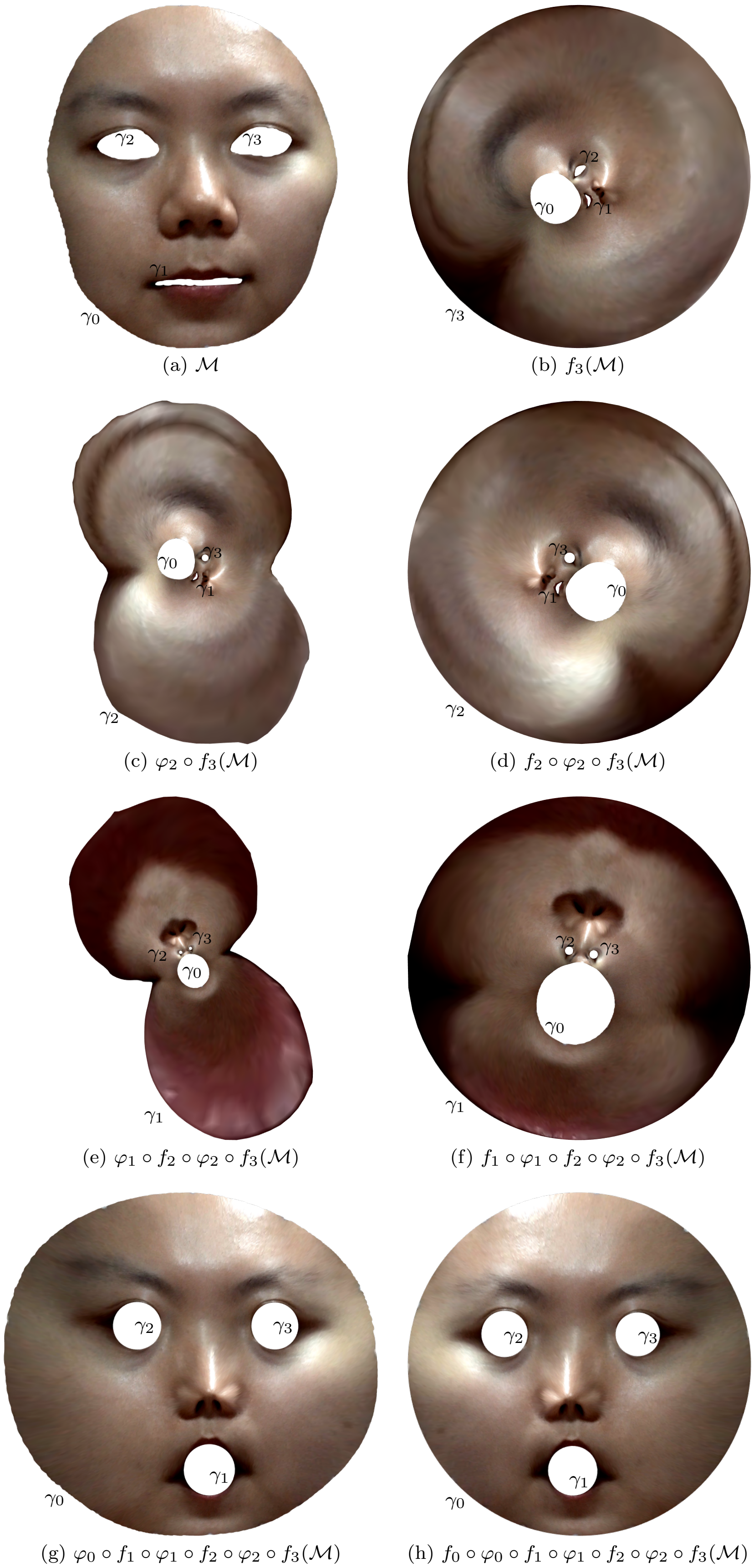

Fig. 1 (a) The model of *Ho's Face with Holes*. (b)-(h) The procedure of Koebe's method proposed by Zeng et al. [29, 30].

Theorem 2 *Let*

$$L = \begin{bmatrix} A & B \\ B^\top & D \end{bmatrix}$$

satisfy the following conditions.

(i) L is a singular and irreducible M-matrix;
(ii) $L\mathbf{1}_{n_L} = 0$;
(iii) B has no zero column vector;
(iv) Both A and D are irreducible.

Let $K = D^{-1}B^\top A^{-1}B$. Then K is positive with $\rho(K) = 1$ being the unique largest eigenvalue of K in modulus.

Proof Applying Lemma 1 to the assumption (i), both A and D are nonsingular M-matrices. Then, by the assumption (iv) and Lemma 3, both A^{-1} and D^{-1} are positive. The assumption (iii) and the positivity of A^{-1} guarantee that $B^\top A^{-1}B$ is positive. Moreover, the positivity of D^{-1} guarantees that $K = D^{-1}(B^\top A^{-1}B)$ is positive. On the other hand, note that $L\mathbf{1}_{n_L} = 0$. That is, $B\mathbf{1}_{n_A} = -A\mathbf{1}_{n_A}$ and $B^\top\mathbf{1}_{n_K} = -D\mathbf{1}_{n_K}$. It follows that

$$\begin{aligned} K\mathbf{1}_{n_K} &= D^{-1}B^\top A^{-1}B\mathbf{1}_{n_K} \\ &= -D^{-1}B^\top A^{-1}A\mathbf{1}_{n_K} \\ &= -D^{-1}B^\top\mathbf{1}_{n_K} \\ &= D^{-1}D\mathbf{1}_{n_K} = \mathbf{1}_{n_K}. \end{aligned}$$

That is, 1 is an eigenvalue of K associated with the eigenvector $\mathbf{1}_{n_K}$. By Lemma 4, $\rho(K) = 1$ is the largest eigenvalue of K with algebraic multiplicity one, and all the other eigenvalues are strictly smaller than 1 in modulus. □

Remark 4 Geometrically, the matrix K, defined as in Theorem 2, maps all the entries of a vector $\mathbf{f}$ to their convex hull. More explicitly, $K\mathbf{1}_{n_K} = \mathbf{1}_{n_K}$ implies that $\sum_{j=1}^{n_K} K_{i,j} = 1$. Also, K is a strictly positive matrix. Hence, for $i = 1, \ldots, n_K$,

$$(K\mathbf{f})_i = \sum_{j=1}^{n_K} K_{i,j}\mathbf{f}_j$$

is a convex combination of the points $\{\mathbf{f}_j \in \mathbb{C}\}_{j=1}^{n_K}$.

In practical applications, the triangular meshes of the simply-connected open surfaces are usually well-conditioned as in Definition 1. Thus, Theorem 2 can be applied.

Corollary 1 *Let $\mathcal{M}$ be a well-conditioned mesh and L be the corresponding Laplacian matrix in a certain vertex ordering as in (9). Let K be the associated matrix defined in (27). Then*

$$\rho(K) = 1 \tag{31}$$

is the largest eigenvalue of K with algebraic multiplicity one, and all the other eigenvalues are strictly smaller than 1 in modulus.

Proof It is shown in Lemma 2 that L is an M-matrix. Note that $\mathcal{M}$ is well-conditioned. The condition (i) in Definition 1 guarantees the irreducibility of L. The conditions (ii) and (iii) in Definition 1 guarantee the irreducibility of the matrices $L_{\mathtt{i},\mathtt{i}}$ and $L_{\mathtt{b},\mathtt{b}}$, respectively. The conditions (iv) in Definition 1 guarantees that every column sum of $L_{\mathtt{i},\mathtt{b}}$ is nonzero. Therefore, by Theorem 2, we obtain the desired results. □

Remark 5 Corollary 1 can be generalized to the Laplacian matrix of weighted graphs with positive weights that satisfies the conditions (i)-(iv) in Definition 1.

In the following, we prove the existence of the accumulation point of the boundary iteration scheme defined by (26).

Theorem 3 *The sequence $\{\mathbf{f}_{\mathtt{b}}^{(k)}\}_{k\in\mathbb{N}}$, defined by (26), has an accumulation point $\mathbf{f}_{\mathtt{b}}^{(*)} \neq \mathbf{1}_{n_{\mathtt{b}}}$ provided that* $\operatorname{rank}(K) \geq 3$ *and $\mathbf{f}_{\mathtt{b}}^{(0)} \neq \mathbf{1}_{n_{\mathtt{b}}}$.*

Proof Since each entry of $\mathbf{f}_\mathtt{b}^{(k)}$ is on the unit circle, by Bolzano-Weierstrass theorem, there exists a vector $\mathbf{f}_\mathtt{b}^{(*)}$ and a convergent subsequence $\{\mathbf{f}_\mathtt{b}^{(k_j)}\}_{j\in\mathbb{N}}$ such that $\lim_{j\to\infty}\mathbf{f}_\mathtt{b}^{(k_j)}=\mathbf{f}_\mathtt{b}^{(*)}$. From Remark 4, the centralization in the iteration (26) and the assumption that $\operatorname{rank}(K)\geq 3$ guarantee that after a rotation by setting $(\mathbf{f}_\mathtt{b}^{(k)})_1=1$ for each $k\in\mathbb{N}$, the maximal argument satisfies

$$\max_{1\leq i\leq n_\mathtt{b}} \operatorname{Arg}\left((CK\mathbf{f}_\mathtt{b}^{(k)})_i\right)>\pi. \tag{32}$$

Otherwise, each entry of the vector $CK\mathbf{f}_\mathtt{b}^{(k)}$ is located on the upper half-plane of $\mathbb{C}$, then the center $\frac{1}{n_K}\sum_{i=1}^{n_K}(CK\mathbf{f}_\mathtt{b}^{(k)})_i\neq 0$ which contradicts that the center should be zero. In particular, Eq. (32) holds for the subsequence $\{k_j\}_{j\in\mathbb{N}}$. Hence, the accumulation point $\mathbf{f}_\mathtt{b}^{(*)}$ satisfies

$$\max_{1\leq i\leq n_\mathtt{b}} \operatorname{Arg}\left((CK\mathbf{f}_\mathtt{b}^{(*)})_i\right)\geq\pi.$$

Therefore, $\mathbf{f}_\mathtt{b}^{(*)}\neq\mathbf{1}_{n_\mathtt{b}}$. □

5 Numerical Experiments

In this section, we demonstrate the numerical results of the conformal parameterizations obtained by CEM algorithm. The maximal number of iterations for CEM algorithm is set to be 20. The linear systems in CEM algorithm are solved using the backslash operator (\) in MATLAB. Also, we compare the efficiency and accuracy of our CEM algorithm to three of the existing state-of-the-art algorithms of conformal parameterizations for simply-connected open surfaces, namely, the heat flow via the quasi-implicit Euler method (QIEM) [16], the fast disk map (FDM) [4], and the linear disk map (LDM) [5]. The MATLAB source code of QIEM is provided by Huang [16]. The MATLAB p-codes of FDM and LDM are obtained from Lui's website [33], respectively. All experiments are performed in MATLAB on a personal laptop with a 2.60GHz CPU and 8GB RAM. Some of the mesh models are obtained from TurboSquid [35], AIM@SHAPE shape repository [32], the Stanford 3D scanning repository [34], and a project page of ALICE [31].

Figures 2-7, respectively, show the models *Left Hand*, *Liu's Neutral Face*, *Liu's Smile Face*, *Liu's Wry Face*, *Liu's Pouting Face* and *Ho's Face with Holes* and their conformal parameterizations computed by CEM algorithm. Fig. 2 indicates that no folding would occur even when the geometry of the surface is a bit complicated. The checkerboard patterns in figures 3-7 indicate that the conformal parameterizations computed by CEM algorithm preserve angles. In addition, Fig. 8 demonstrates the relationship between the number of iterations and the conformal energy $\mathcal{E}_C(\mathbf{f})$ for (a) *Chinese Vase*, (b) *Bourbon Bottle*, (c) *David Head* and (d) *Human Brain*. These results indicate that the proposed boundary iteration scheme (26) for CEM performs well in decreasing the conformal energy. Furthermore, Fig. 9 shows the histograms of the angular distortion (counted in degree) of the conformal parameterizations obtained by CEM algorithm for (a) *Liu's Neutral Face*, (b) *Liu's Smile Face*, (c) *Liu's Wry Face* and (d) *Liu's Pouting Face*. Here, the angular distortion refers as to the absolute value of the difference (counted in degree) between angles of the triangle elements on the mesh model and the corresponding angles on the conformal parameterization. As shown in Fig. 9, most of the angular distortions are less than one degree, which is quite satisfactory.

A comparison of the computational cost between QIEM, FDM, LDM and CEM algorithm is demonstrated in Table 1. Also, Fig. 10 illustrates the relationship between the number of faces and the the computational cost. To measure how much CEM algorithm is more efficient than QIEM/FDM/LDM, we define the rate of the speedup by

$$\text{rate of speedup}=\frac{\text{computational time of QIEM/FDM/LDM}}{\text{computational time of CEM}}-1. \tag{33}$$

A positive rate of speedup indicates that CEM algorithm is more efficient than QIEM/FDM/LDM. According to Table 2, CEM algorithm always has a better efficiency than QIEM/FDM/LDM with the average rate of the speedup 8.5/17.2/4.1. In other words, CEM algorithm saves about 89%/94%/80% of the computational time of QIEM/FDM/LDM in average.

Furthermore, comparisons of the conformality distortion in terms of the conformal energy and the angular distortion for the parameterization map $\mathbf{f}$ are demonstrated in Table 3 and Table 4, respectively. In general, as shown in figures 11 and 12, both the conformal energy and the standard deviation of angular distortions

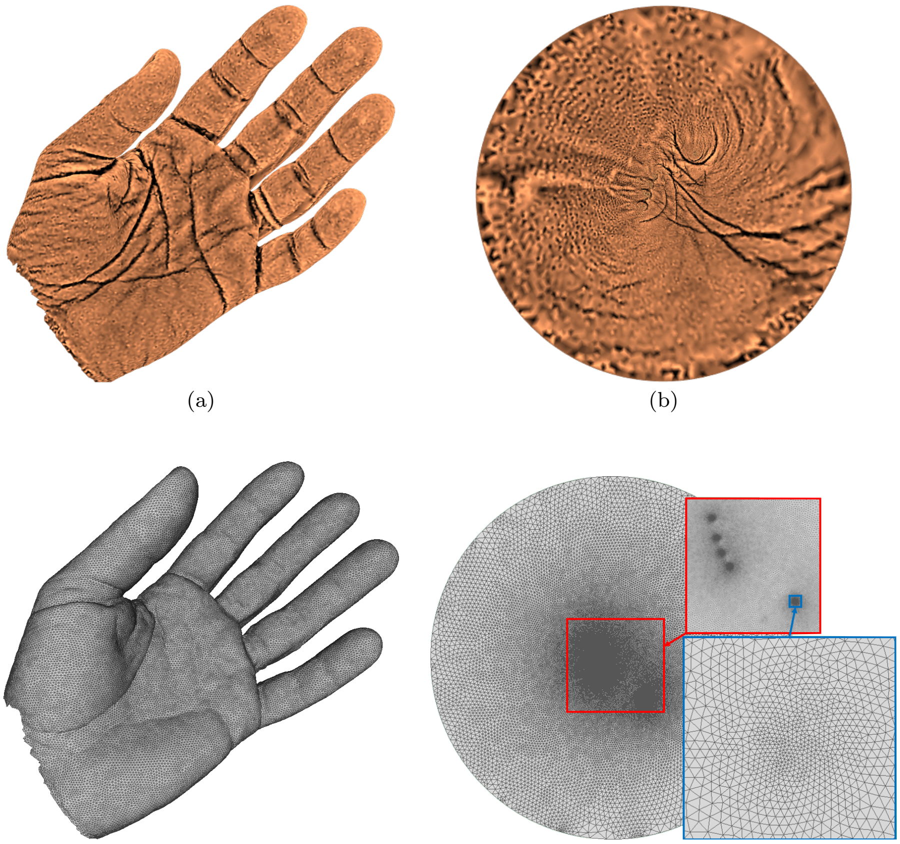

(a) (b) (c) (d)

Fig. 2 (a) The *Left Hand* model. (b) The conformal parameterization obtained by CEM algorithm in which the color represents the mean curvature of the surface. (c) The mesh of the model. (d) The mesh of the conformal parameterization obtained by CEM algorithm.

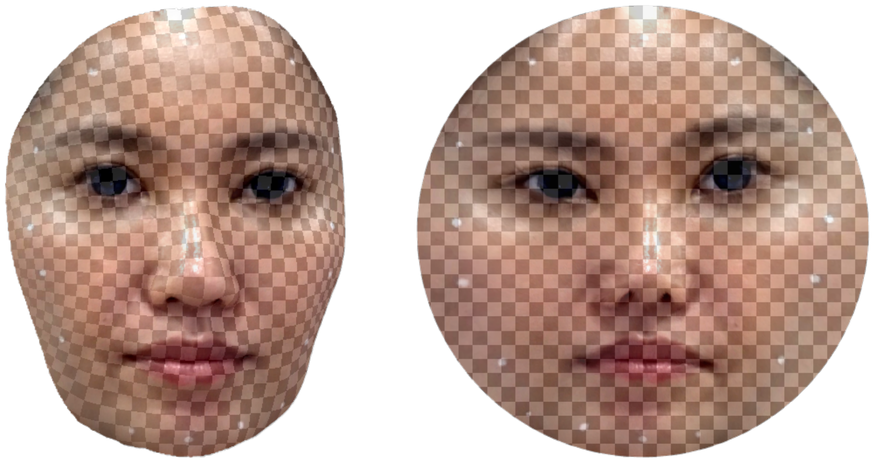

(a) (b)

Fig. 3 (a) The model of *Liu's Neutral Face*. (b) The conformal parameterization obtained by CEM algorithm.

(a) (b)

Fig. 4 (a) The model of *Liu's Smile Face.* (b) The conformal parameterization obtained by CEM algorithm.

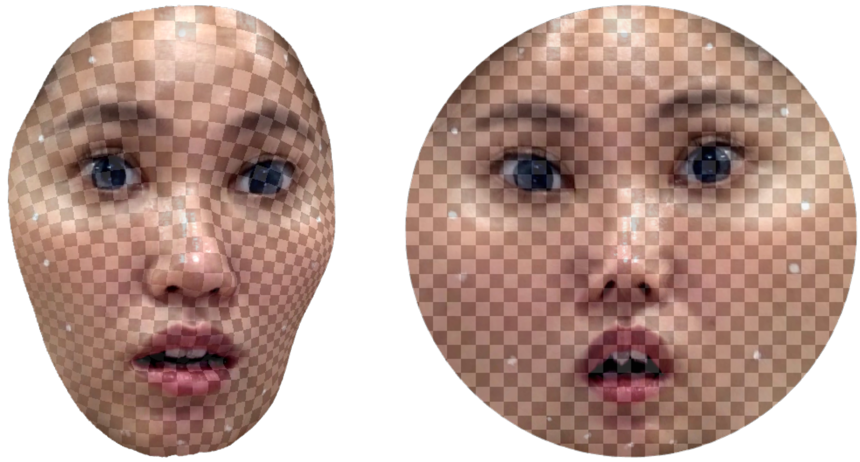

(a) (b)

Fig. 5 (a) The model of *Liu's Wry Face.* (b) The conformal parameterization obtained by CEM algorithm.

(a) (b)

Fig. 6 (a) The model of *Liu's Pouting Face.* (b) The conformal parameterization obtained by CEM algorithm.

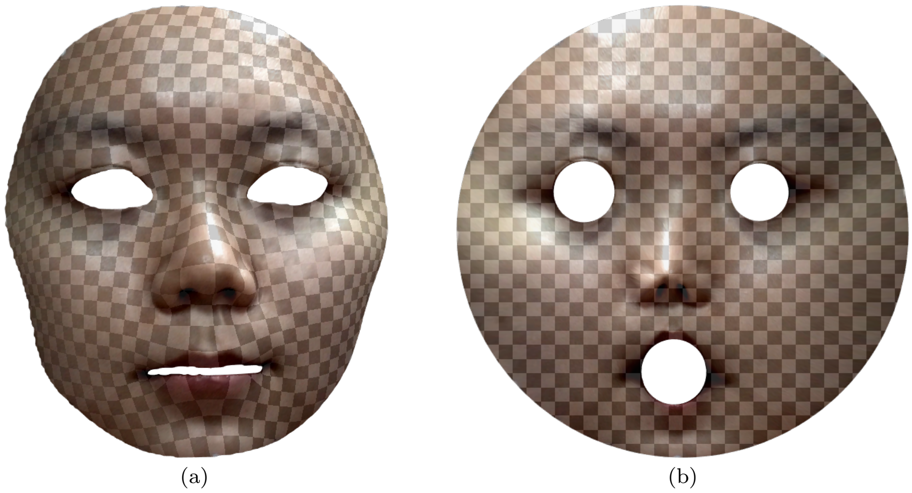

Fig. 7 (a) The model of *Ho's Face with Holes*. (b) The conformal parameterization obtained by the generalized CEM algorithm.

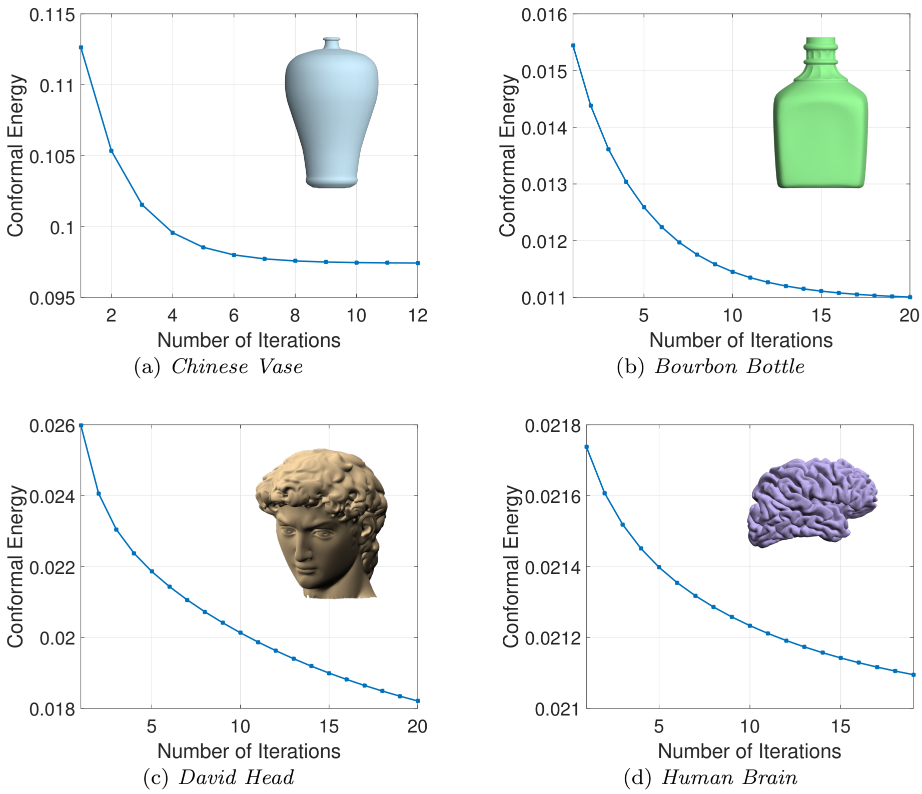

Fig. 8 The relationship between the number of iterations and the conformal energy of the parameterization obtained by CEM algorithm for (a) *Chinese Vase*, (b) *Bourbon Bottle*, (c) *David Head* and (d) *Human Brain*.

produced by FDM, LDM and CEM are similar. On the other hand, the mean of angular distortions by FDM and LDM are slightly better than that of CEM.

In summary, the CEM algorithm has a better efficiency than the existing state-of-the-art algorithms [16, 4, 5] that saves more than 80% of computational cost on average while producing the similar conformal energy and the angular distortion.

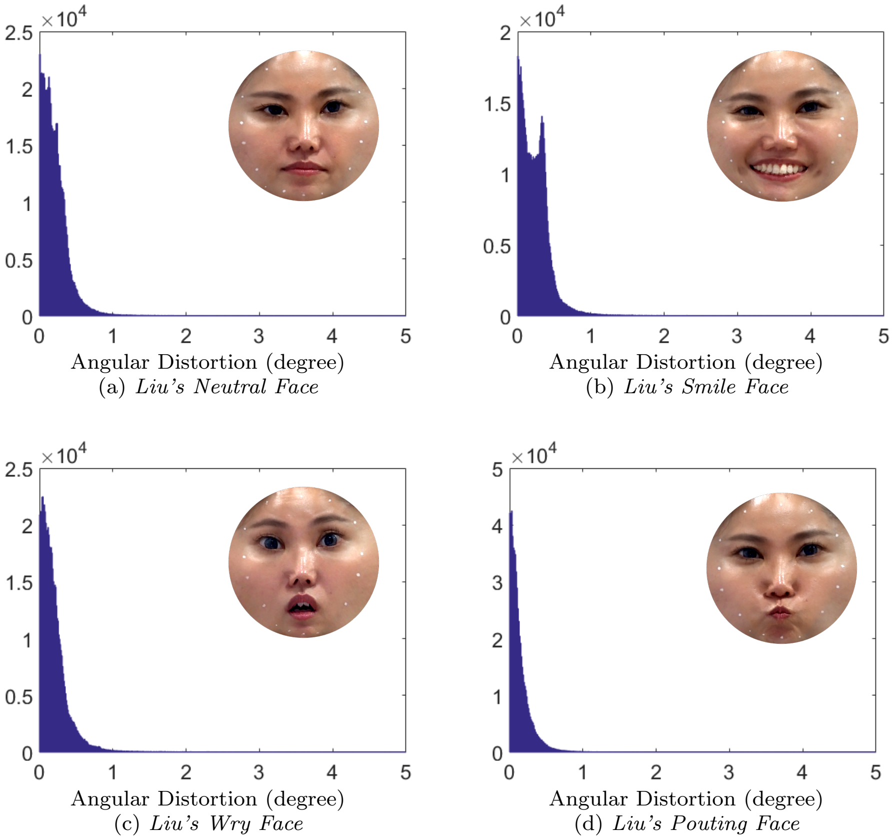

(a) *Liu's Neutral Face* (b) *Liu's Smile Face*

(c) *Liu's Wry Face* (d) *Liu's Pouting Face*

Fig. 9 The histograms of the angular distortions (degree) of the conformal parameterizations obtained by CEM algorithm for (a) *Liu's Neutral Face*, (b) *Liu's Smile Face*, (c) *Liu's Wry Face* and (d) *Liu's Pouting Face*. Note that the angular distortion refers as to the absolute value of the difference (counted in degree) between the angle on the mesh model and the disk.

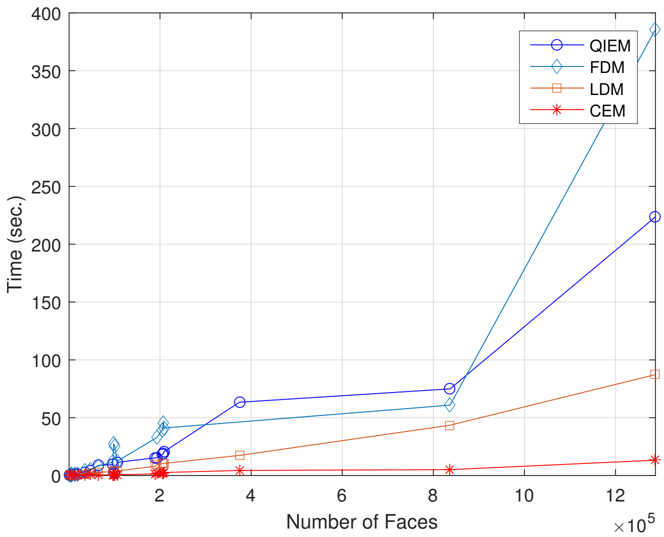

Fig. 10 Computational cost (sec.) vs number of faces by QIEM, FDM, LDM, and CEM.

Geometric Model	No. of Faces	QIEM [16]	FDM [4]	LDM [5]	CEM	
					Time	#Iter.
Nefertiti	562	0.04	0.08	0.30	0.03	19
Cowboy Hat	4,604	0.35	0.35	0.13	0.02	1
Chinese Vase	5,592	0.18	0.81	0.13	0.06	12
Bourbon Bottle	13,088	1.08	0.87	0.37	0.27	20
Foot	19,966	1.49	1.05	0.54	0.35	15
Chinese Lion	34,421	3.09	4.16	1.15	0.45	13
David Head	47,280	4.47	5.33	1.63	0.98	20
Stanford Bunny	65,221	8.78	8.36	2.65	0.53	1
Human Brain	96,811	9.46	11.73	3.59	0.68	19
Ho's Pouting Face	98,316	2.50	27.32	3.86	0.58	5
Ho's Neutral Face	100,675	2.18	25.36	4.40	0.45	1
Left Hand	105,860	11.38	12.35	3.88	0.72	2
Statue of Liberty	190,162	15.33	–	8.03	1.38	1
Liu's Neutral Face	193,298	15.36	32.81	9.47	2.01	2
Liu's Smile Face	205,207	18.16	39.61	10.35	1.85	1
Liu's Pouting Face	207,721	19.18	45.89	10.47	1.79	3
Liu's Wry Face	208,283	20.47	41.08	10.44	2.62	3
Isis Statue	374,309	63.35	–	17.39	4.38	5
Bimba Statue	836,740	74.92	60.86	43.51	5.10	2
Knit Cap Man	1,287,579	223.58	385.70	87.28	13.27	1

Table 1 Computational cost (sec.) for computing conformal parameterizations by QIEM, FDM, LDM, and CEM algorithms.

Geometric Model	No. of Vertices	No. of Faces	QIEM [16]	FDM [4]	LDM [5]
Nefertiti	299	562	0.33	1.67	9.00
Cowboy Hat	2,327	4,604	16.50	16.50	5.50
Chinese Vase	2,809	5,592	2.00	12.50	1.17
Bourbon Bottle	6,569	13,088	3.00	2.22	0.37
Foot	10,010	19,966	3.26	2.00	0.54
Chinese Lion	17,334	34,421	5.87	8.24	1.56
David Head	23,889	47,280	3.56	4.44	0.66
Stanford Bunny	32,717	65,221	15.57	14.77	4.00
Human Brain	48,463	96,811	12.91	16.25	4.28
Ho's Pouting Face	49,596	98,316	3.31	46.10	5.66
Ho's Neutral Face	50,779	100,675	3.84	55.36	8.78
Left Hand	53,054	105,860	14.81	16.15	4.39
Statue of Liberty	95,283	190,162	10.11	–	4.82
Liu's Neutral Face	97,264	193,298	6.64	15.31	3.71
Liu's Smile Face	103,230	205,207	8.82	20.41	4.59
Liu's Pouting Face	104,497	207,721	9.72	24.64	4.85
Liu's Wry Face	104,786	208,283	6.81	14.68	2.98
Isis Statue	187,277	374,309	13.46	–	2.97
Bimba Statue	418,951	836,740	13.69	10.93	7.53
Knit Cap Man	644,029	1,287,579	15.85	29.07	5.58

Table 2 The rate of speedup of CEM algorithm with respect to QIEM, FDM, and LDM, defined by Eq. (33).

6 Applications on Surface Morphing

Surface morphing is a process of smoothly transforming a surface into another one. In general, a good morphing path should be smooth and shape preserving. In other words, every vertex has no weird movement and the topology of surfaces does not change during the morphing process. Also, the selected landmarks on each surface remain matched. Technically, as shown in Fig. 13, a morphing sequence between two discrete surfaces $\mathcal{M}$ and $\mathcal{N}$ can be obtained by a cubic spline homotopy via a smooth bijective map $r : \mathcal{M} \to \mathcal{N}$, which is called a *registration map*. However, it is usually not easy to find a registration map between two surfaces in the space $\mathbb{R}^3$. Thanks to the bijectivity of conformal parameterizations $f : \mathcal{M} \to \mathbb{D}$ and $g : \mathcal{N} \to \mathbb{D}$, the problem can be reduced into finding a registration map between two unit disks $f(\mathcal{M})$ and $g(\mathcal{N})$. In the linear discretization, the conformal parameterizations f and g can be expressed by the vectors $\mathbf{f} \in \mathbb{C}^{n_\mathtt{f}}$ and $\mathbf{g} \in \mathbb{C}^{n_\mathtt{g}}$, respectively. Suppose $\mathtt{f}$ and $\mathtt{g}$ denote ordered index sets of the selected landmarks on $\mathbf{f}$ and $\mathbf{g}$, respectively. When the correspondence of the landmark pairs $\{((\mathbf{f}_\mathtt{f})_j, (\mathbf{g}_\mathtt{g})_j)\}_{j=1}^{n_\mathtt{f}}$ is taken into

Geometric Model	No. of Faces	QIEM [16]	FDM [4]	LDM [5]	CEM Alg.
Nefertiti	562	0.0264	0.0242	0.0337	0.0278
Cowboy Hat	4,604	0.0067	0.0030	0.0039	0.0031
Chinese Vase	5,592	0.0986	0.0974	0.1141	0.0974
Bourbon Bottle	13,088	0.0110	0.0110	0.0112	0.0111
Foot	19,966	0.0228	0.0121	0.0165	0.0120
Chinese Lion	34,421	0.0139	0.0139	0.0140	0.0143
David Head	47,280	0.0309	0.0157	0.0172	0.0197
Stanford Bunny	65,221	0.0172	0.0173	0.0168	0.0172
Human Brain	96,811	0.0220	0.0213	0.0233	0.0224
Ho's Pouting Face	98,316	0.0030	0.0028	0.0032	0.0030
Ho's Neutral Face	100,675	0.0024	0.0023	0.0045	0.0022
Left Hand	105,860	0.0110	0.0110	0.0104	0.0102
Statue of Liberty	190,162	0.0038	–	0.0038	0.0036
Liu's Neutral Face	193,298	0.0031	0.0031	0.0032	0.0032
Liu's Smile Face	205,207	0.0033	0.0033	0.0035	0.0033
Liu's Pouting Face	207,721	0.0037	0.0037	0.0038	0.0038
Liu's Wry Face	208,283	0.0038	0.0038	0.0038	0.0038
Isis Statue	374,309	0.0374	–	0.0108	0.0101
Bimba Statue	836,740	0.0023	0.0237	0.0023	0.0024
Knit Cap Man	1,287,579	0.0108	0.0111	0.0117	0.0114

Table 3 The conformal energy $\mathcal{E}_C$ of the parameterizations $\mathbf{f}$ obtained by QIEM, FDM, LDM, and CEM algorithms.

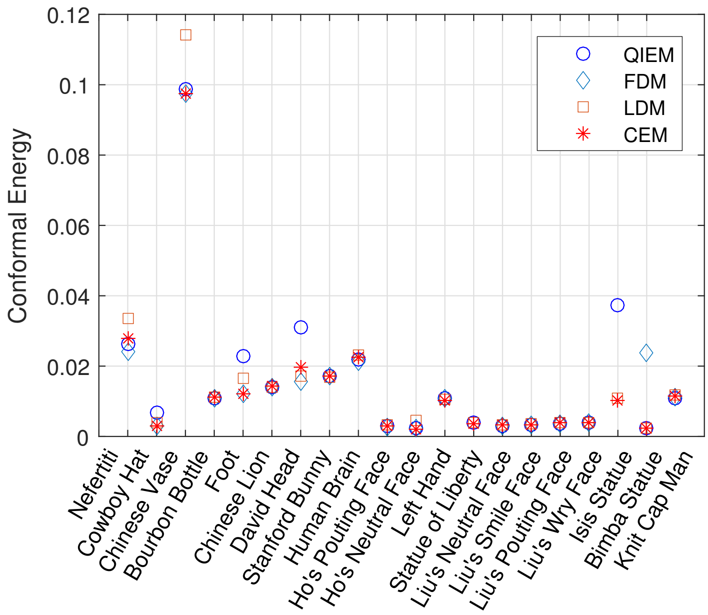

Fig. 11 The conformal energy $\mathcal{E}_C$ of the parameterizations $\mathbf{f}$ computed by QIEM, FDM, LDM, and CEM algorithms.

account, the registration map between two unit disks can be obtained by minimizing the *registration energy functional* defined by

$$\mathcal{E}_R(\mathbf{f}) = \mathcal{E}_D(\mathbf{f}) + \lambda \sum_{j=1}^{n_{\mathtt{m}}} |(\mathbf{f}_{\mathtt{f}})_j - (\mathbf{g}_{\mathtt{g}})_j|^2. \tag{34}$$

An illustration for the construction of the registration maps between three human faces of different facial expressions via the conformal parameterizations is shown in Fig. 14. Let $\mathcal{M}_1$, $\mathcal{M}_2$ and $\mathcal{M}_3$ be the geometric models of *Liu's Wry Face*, *Liu's Neutral Face* and *Liu's Smile Face*, respectively. As illustrated in Fig. 14, the corresponding conformal parameterization maps obtained by CEM algorithm are denoted as f_1, f_2 and f_3, respectively. The Möbius transform m_1 maps the landmark at nose to the center of the disk. The registration maps r_2 and r_3 are, respectively, obtained by minimizing the registration energy functional (34) with the given pairs of landmarks. As a result, $r_2^{-1} \circ m_1 \circ f_1$ forms a registration map between $\mathcal{M}_1$ and $\mathcal{M}_2$. Similarly, $r_3^{-1} \circ m_1 \circ f_1$ and $r_3^{-1} \circ r_2$ form registration maps between $\mathcal{M}_1$ and $\mathcal{M}_3$, as well as,

Geometric Model	QIEM [16]		FDM [4]		LDM [5]		CEM	
	Mean	SD	Mean	SD	Mean	SD	Mean	SD
Nefertiti	2.53	3.38	2.48	3.36	2.79	3.46	2.65	3.35
Cowboy Hat	1.61	1.28	0.87	1.03	0.98	1.10	0.90	1.03
Chinese Vase	4.49	5.03	4.50	5.02	4.76	4.99	4.50	5.02
Bourbon Bottle	2.23	2.21	2.18	2.21	2.21	2.21	2.19	2.20
Foot	2.56	1.85	1.41	1.13	1.42	1.16	1.41	1.14
Chinese Lion	1.42	2.04	1.42	2.04	1.42	2.05	1.49	2.06
David Head	4.28	5.91	3.06	5.86	3.11	5.86	3.24	5.84
Stanford Bunny	1.68	3.83	1.08	1.79	1.08	1.79	1.08	1.79
Human Brain	1.87	1.72	1.46	1.59	1.46	1.59	1.49	1.60
Ho's Pouting Face	0.34	1.49	0.35	1.49	0.35	1.49	0.36	1.49
Ho's Neutral Face	0.32	1.38	0.32	1.41	0.37	1.38	0.42	1.38
Left Hand	6.41	14.71	1.21	1.31	1.21	1.31	1.23	1.32
Statue of Liberty	2.84	10.89	–	–	1.22	2.59	2.38	2.57
Liu's Neutral Face	0.25	2.01	0.25	1.99	0.25	2.01	0.35	2.01
Liu's Smile Face	0.27	2.10	0.27	2.08	0.27	2.10	0.39	2.09
Liu's Pouting Face	0.28	2.25	0.27	2.23	0.28	2.25	0.30	2.25
Liu's Wry Face	0.30	2.25	0.30	2.23	0.30	2.25	0.37	2.25
Isis Statue	5.13	4.26	–	–	0.41	0.62	0.43	0.63
Bimba Statue	0.45	1.00	1.50	2.13	0.34	0.97	0.42	0.97
Knit Cap Man	1.18	1.29	0.53	0.91	0.59	0.91	0.93	0.99

Table 4 The angular distortion of the conformal parameterizations obtained by QIEM, FDM, LDM, and CEM algorithms.

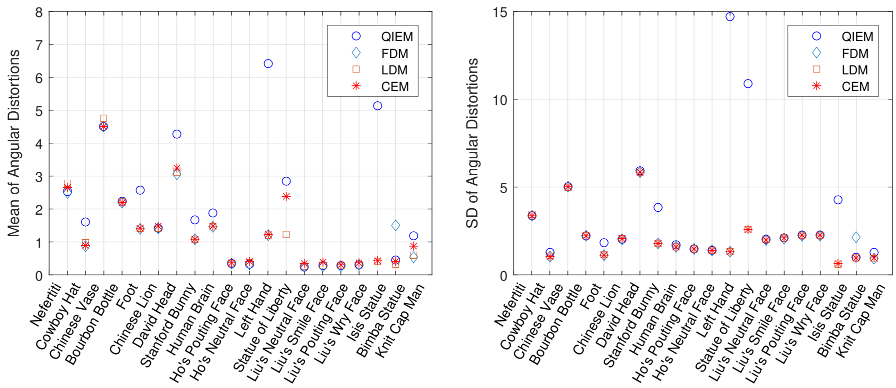

Fig. 12 The (a) mean and (b) standard deviation of the angular distortion of the conformal parameterizations computed by QIEM, FDM, LDM, and CEM algorithms.

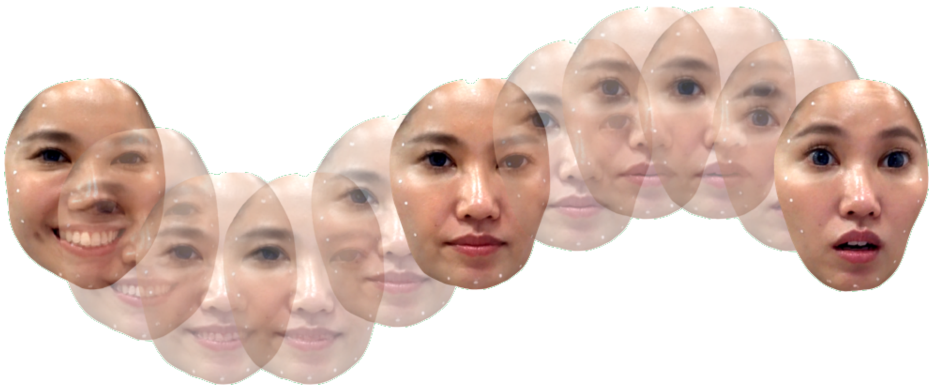

Fig. 13 An illustration of the cubic spline homotopy between human faces of three different facial expressions.

Fig. 14 An illustration to the construction of the registration maps between three human faces of different facial expressions via the conformal parameterizations.

$\mathcal{M}_2$ and $\mathcal{M}_3$, respectively. A demo video of the surface morphing in three different views can be found at https://youtu.be/fgcCu-pz2vY.

7 Conclusions

In this paper, we have proposed an efficient CEM algorithm for computing conformal parameterizations of simply-connected open surfaces. Our numerical results indicate that a conformal parameterization can be computed in less than one second for a mesh model of more than 100,000 triangular elements by CEM algorithm. Also, we generalize the proposed CEM algorithm for the computation of conformal parameterizations of multiply-connected surfaces. The existence of a nontrivial accumulation point of CEM algorithm is guaranteed. An application to the surface morphing between simply-connected open surfaces using conformal parameterizations is demonstrated. Thanks to the efficiency and robustness of CEM algorithm, the whole computation of the surface morphing can be performed efficiently. Such encouraging results build the confidence of the power of the CEM algorithm on the real-time applications of conformal parameterizations.

Acknowledgments The authors want to thank Yen-Jen Cheng, Dr. Wei-Qiang Huang, and Dr. Ching-Sung Liu for useful discussions and thank Prof. So-Hsiang Chou for the help on polishing the manuscript.

They also want to thank the anonymous referees for their valuable comments and suggestions. The 3D scanner and camera devices are supported by the ST Yau Center in Taiwan. This work is partially supported by the Ministry of Science and Technology, the National Center for Theoretical Sciences, the Taida Institute for Mathematical Sciences, and the ST Yau Center in Taiwan.

References

1. Angenent, S., Haker, S., Tannenbaum, A., Kikinis, R.: On the Laplace-Beltrami operator and brain surface flattening. IEEE Trans. Med. Imaging **18**(8), 700–711 (1999)
2. Berman, A., Plemmons, R.: Nonnegative Matrices in the Mathematical Sciences. Society for Industrial and Applied Mathematics (1994)
3. Choi, P.T., Lam, K.C., Lui, L.M.: FLASH: Fast landmark aligned spherical harmonic parameterization for genus-0 closed brain surfaces. SIAM J. Imaging Sci. **8**(1), 67–94 (2015)
4. Choi, P.T., Lui, L.M.: Fast disk conformal parameterization of simply-connected open surfaces. J. Sci. Comput. **65**(3), 1065–1090 (2015)
5. Choi, P.T., Lui, L.M.: A linear algorithm for disk conformal parameterization of simply-connected open surfaces (2015). Arxiv:1508.00396v1
6. Desbrun, M., Meyer, M., Alliez, P.: Intrinsic parameterizations of surface meshes. Comput. Graph. Forum **21**(3), 209–218 (2002)
7. Floater, M.S., Hormann, K.: Surface parameterization: a tutorial and survey. Advances in multiresolution for geometric modelling. Springer Berlin Heidelberg pp. 157–186 (2005)
8. Golub, G.H., Van Loan, C.F.: Matrix Computations. Johns Hopkins Univ. Press (1996)
9. Gu, D.X., Luo, F., Yau, S.T.: Fundamentals of computational conformal geometry. Math. Comput. Sci. **4**(4), 389–429 (2010)
10. Gu, X., Wang, Y., Chan, T.F., Thompson, P.M., Yau, S.T.: Genus zero surface conformal mapping and its application to brain surface mapping. IEEE Trans. Med. Imaging **8**, 949–958 (2004)
11. Gu, X., Yau, S.T.: Computational Conformal Geometry, 1 edn. Higher Education Press (2008)
12. Gu, X.D., Zeng, W., Luo, F., Yau, S.T.: Numerical computation of surface conformal mappings. Comput. Methods Funct. Theory **11**(2), 747–787 (2011)
13. Haker, S., Angenent, S., Tannenbaum, A., Kikinis, R., Sapiro, G., Halle, M.: Conformal surface parameterization for texture mapping. IEEE Trans. Vis. Comput. Graph. (2), 181–189 (2000)
14. Hormann, K., Lévy, B., Sheffer, A.: Mesh parameterization: Theory and practice. In: ACM SIGGRAPH Course Notes (2007). DOI 10.1145/1281500.1281510
15. Horn, R.A., Johnson, C.: Matrix Analysis. Cambridge University Press (1990)
16. Huang, W.Q., Gu, X.D., Huang, T.M., Lin, S.S., Lin, W.W., Yau, S.T.: High performance computing for spherical conformal and Riemann mappings. Geom. Imag. Comput. **1**(2), 223–258 (2014)
17. Huang, W.Q., Gu, X.D., Lin, W.W., Yau, S.T.: A novel symmetric skew-hamiltonian isotropic Lanczos algorithm for spectral conformal parameterizations. J. Sci. Comput. **61**(3), 558–583 (2014)
18. Hurdal, M.K., Bowers, P.L., Stephenson, K., Sumners, D.W.L., Rehm, K., Schaper, K., Rottenberg, D.A.: Quasi-conformally flat mapping the human cerebellum. Med. Image Comput. Comput. Assist. Interv. pp. 279–286 (1999). DOI 10.1007/10704282_31
19. Hutchinson, J.E.: Computing conformal maps and minimal surfaces. Proc. Centre Math. Appl. **26**, 140–161 (1991)
20. Molitierno, J.J.: Applications of Combinatorial Matrix Theory to Laplacian Matrices of Graphs. CRC Press (2012)
21. Mullen, P., Tong, Y., Alliez, P., Desbrun, M.: Spectral conformal parameterization. Comput. Graph. Forum **27**(5), 1487–1494 (2008)
22. Pinkall, U., Polthier, K.: Computing discrete minimal surfaces and their conjugates. Exp. Math. **2**, 15–36 (1993)
23. Reuter, M., Biasotti, S., Giorgi, D., Patanè, G., Spagnuolo, M.: Discrete Laplace-Beltrami operators for shape analysis and segmentation. Comput. Graph. **33**(3), 381–390 (2009)
24. Sheffer, A., Lévy, B., Mogilnitsky, M., Bogomyakov, A.: ABF++: Fast and robust angle based flattening. ACM Trans. Graph. **24**(2), 311–330 (2005)
25. Sheffer, A., Praun, E., Rose, K.: Mesh parameterization methods and their applications. Found. Trends. Comp. Graphics and Vision. **2**(2), 105–171 (2006)

26. Sheffer, A., de Sturler, E.: Parameterization of faceted surfaces for meshing using angle-based flattening. Eng. with Comput. **17**(3), 326–337 (2001)
27. Stephenson, K.: The approximation of conformal structures via circle packing. In: Computational Methods and Function Theory 1997, Proceedings of the Third CMFT conference, pp. 551–582. World Scientific (1999)
28. Yau, S.T., Schoen, R.: Lectures on Differential Geometry. International Press (2010)
29. Zeng, W., Lui, L.M., Gu, X., Yau, S.T.: Shape analysis by conformal modules. Methods Appl. Anal. **15**(4), 539–556 (2008)
30. Zeng, W., Yin, X., Zhang, M., Luo, F., Gu, X.: Generalized koebe's method for conformal mapping multiply connected domains. In: 2009 SIAM/ACM Joint Conference on Geometric and Physical Modeling, pp. 89–100. ACM (2009)
31. ALICE. http://alice.loria.fr/
32. Digital Shape Workbench - Shape Repository. http://visionair.ge.imati.cnr.it/ontologies/shapes/
33. LokMingLui.com. http://www.math.cuhk.edu.hk/~lmlui/
34. The Stanford 3D Scanning Repository. http://graphics.stanford.edu/data/3Dscanrep/
35. TurboSquid. http://www.turbosquid.com/